

A Comprehensive Study on Reliability Performance of Photovoltaic-Battery-Based Microgrids under Different Energy Management Strategies

Jiang, Jiahui; Peyghami, Saeed; Coates, Colin; Blaabjerg, Frede

Published in:
Journal of Energy Storage

DOI (link to publication from Publisher):
[10.1016/j.est.2021.103051](https://doi.org/10.1016/j.est.2021.103051)

Creative Commons License
CC BY 4.0

Publication date:
2021

Document Version
Publisher's PDF, also known as Version of record

[Link to publication from Aalborg University](#)

Citation for published version (APA):
Jiang, J., Peyghami, S., Coates, C., & Blaabjerg, F. (2021). A Comprehensive Study on Reliability Performance of Photovoltaic-Battery-Based Microgrids under Different Energy Management Strategies. *Journal of Energy Storage*, 43, Article 103051. <https://doi.org/10.1016/j.est.2021.103051>

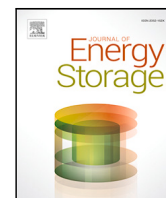
General rights

Copyright and moral rights for the publications made accessible in the public portal are retained by the authors and/or other copyright owners and it is a condition of accessing publications that users recognise and abide by the legal requirements associated with these rights.

- Users may download and print one copy of any publication from the public portal for the purpose of private study or research.
- You may not further distribute the material or use it for any profit-making activity or commercial gain
- You may freely distribute the URL identifying the publication in the public portal -

Take down policy

If you believe that this document breaches copyright please contact us at vbn@aub.aau.dk providing details, and we will remove access to the work immediately and investigate your claim.



A comprehensive study on reliability performance of Photovoltaic-battery-based microgrids under different energy management strategies

Jiahui Jiang^a, Saeed Peyghami^{b,*}, Colin Coates^a, Frede Blaabjerg^b

^a School of Electrical Engineering and Computing, University of Newcastle, Callaghan NSW 2308, Australia

^b Department of AAU Energy, Aalborg University, Aalborg 9220 Ost, Denmark

ARTICLE INFO

Keywords:

Energy storage
Energy management strategy
Reliability analysis
Microgrid
Distributed generation
PV systems

ABSTRACT

As the demand for power reliability keeps rising in modern society, the integration of energy storage systems into power networks increases at an unprecedented rate. Meanwhile, reliability analysis and enhancement of a power network attracts more and more attention. This paper explores the impact of four different energy management strategies (EMSs) on the reliability of microgrids, which play an important role in future distribution networks. The reliability performance is analysed on different levels, including converter interfaces and battery storage units on device level as well as power supply reliability on system level. The numerical analysis has shown that the employed EMS can remarkably affect the reliability indices of the system. The battery lifetime can be increased by more than 50% and annual energy loss can be reduced by up to 92%. Since the economic decision-making depends on the components lifetime and overall system performance, this paper provides deep insights for power engineers to properly design, plan and control future microgrids.

1. Introduction

Distributed generations (DG) has facilitated decarbonization by revolutionizing power systems. Among different types of DG, renewable energy sources (RES) and energy storage systems (ESS) compose a large portion [1]. Supportive policies, maturing technologies and sharp cost reductions are enabling RES to be more accessible. Solar Photovoltaic (PV) is consistently cheaper than new coal/gas fired power plants in most parts of the world [2]. However, its intermittent and uncertain power generation is inevitable. An ESS connected solar system is an effective option to improve system resilience. Compared to a centralized power generation plant, the location of DG is relatively flexible and geographically distributed. These features allow a group of DG to form a standalone network supporting local power demand, namely, microgrid (MG) [3]. The main advantages of MG operation is that it can improve the power reliability for local loads [4]. For instance, a grid-connected MG can be disconnected from the utility and operate autonomously after a grid fault [5].

Among all types of ESS, batteries are suitable in many applications because of their relatively high quality in both power density and energy density [6]. The high cost of batteries is, however, one of the major concerns towards de-carbonization. Hence, battery reliability remains a heated topic for decades. The lifetime of a battery is closely

related to its charging & discharging mechanism and state of charge (SOC) [7]. Power management and energy management of batteries thus play an important role in battery reliability. Meanwhile, most DG units interface with the grid through power-electronic devices. The lifetime consumption of employed power electronics is also affected by the energy management strategy (EMS) [4]. It can be seen that the reliability of MG components is closely related with the adopted EMS.

Energy management is the issue of optimal energy distribution targeting different objectives subject to various constraints. In MG energy management, the commonly considered objectives are reducing overall energy cost [8–15], increasing renewable penetration level [16], minimizing environmental pollution [17,18], effectively responding to weather changes [19], voltage and frequency regulation [20–22], reliability improvement [8,23] and so on. The optimization scheme developed in [9] addressed the intrinsically stochastic availability of RES with battery storage and minimized the overall cost for microgrids with a high penetration of RES. The optimal control strategy in [15] considers the real-time system electricity pricing of both utility grid and DG, in order to reduce the operation and consumption cost. Smart metering technology is also integrated in the optimization algorithm in [24]. An off-line strategy through an online algorithm method is implemented in [14] to manage power flow among the storage system,

* Corresponding author.

E-mail address: sap@et.aau.dk (S. Peyghami).

<https://doi.org/10.1016/j.est.2021.103051>

Received 3 May 2021; Received in revised form 10 July 2021; Accepted 30 July 2021

Available online 8 September 2021

2352-152X/© 2021 The Author(s). Published by Elsevier Ltd. This is an open access article under the CC BY license (<http://creativecommons.org/licenses/by/4.0/>).

DG and an aggregated load, with the aim of minimizing total energy cost. The two-level algorithm in [22] employs machine learning on first-level to minimize cost and user dissatisfaction level and proposes transactive energy management on second-level to regulate voltage and current, prevent rebound peak effect with low computational burden. Probabilistic forward-backward load flow is used in [23] to minimize energy cost while considering technical criteria such as voltage profile and reliability. The reliability index employed in the study is based on system failure rate and duration.

From the literature review above, it can be clearly seen that the studied EMS mostly over simplify or ignore the reliability performance of the MG. The existing studies on MG reliability are also limited. In [25], the improving effect of decentralized control architecture on system reliability is validated by using Markov chain models. On the other hand, [26] investigates the reliability on device level, AC-DC converters, under different topological structures and modulation strategies. Study [27] aims to assess overall reliability of an islanded MG through a holistic operation failure rate model. However, the employed EMS is not clear. Although [28] aims to improve the overall system reliability, the analysis is based on one single EMS for an islanded MG. Since the EMS impacts on the operation of batteries, the interfacing converters and the interaction between different elements, a thorough reliability study, both at device level and system level, is needed.

In addition, most existing EMS objectives are proposed at the MG system level. With internal energy transactions occurring within the MG, the evaluation at unit level is worth discussing too. Study in [16] considers the operation costs for each prosumer based on the proposed optimal peer-to-peer energy transaction. It gives a better understanding of the benefits for each prosumer. However, the life cycle cost evaluation on the employed components is overly simplified.

This paper establishes the link between MG EMS and reliability assessment. In the context of a PV-battery-based MG, the power reliability can be studied from different perspectives: lifetime consumption of batteries, ageing of power electronic devices due to thermal damage, and loss of load due to generation uncertainty or contingencies. The battery lifetime consumption can be obtained from battery cycle life model and its power flow profiles [7]. The thermal damage of power electronics is closely related to its thermal cycling, according to physics of failure (POF) analysis [29,30]. Since PV panels and batteries connect to the grid through power converters, the ageing of converters is analysed in this paper [31]. According to [32,33], the thermal damage analysis can be conducted based on device models (the most vulnerable components) and corresponding long-term mission profiles. As for loss of load analysis, Monte Carlo simulations can be applied to different power sources with a specified outage rate. The power flow can be obtained under different operation conditions and the amount of load loss is used to assess power reliability.

The intention of this paper is to help power engineers to have a deeper insight into the system performance at different levels, which can facilitate optimal and cost-effective design, planning, control, operation and maintenance of future distributed power networks. The main contributions of this paper are:

- The reliability performance of a PV-battery-based MG is analysed under different EMSs.
- A comprehensive reliability assessment method is studied, including battery lifetime consumption, converter ageing and overall system reliability.
- The effects of EMS on each participating unit are also discussed.

The process of reliability assessment for a power system is shown in Fig. 1. The rest of the paper is structured as per the flowchart. Section 2 demonstrates four different EMSs for a community MG. The reliability models of a battery, a power converter and a system are built in Section 3. Numerical studies are conducted in Section 4 based on annual mission profiles of the MG sources and loads. It is followed by the reliability analysis from different perspectives presented in Section 5. Finally, the conclusions are drawn in Section 6.

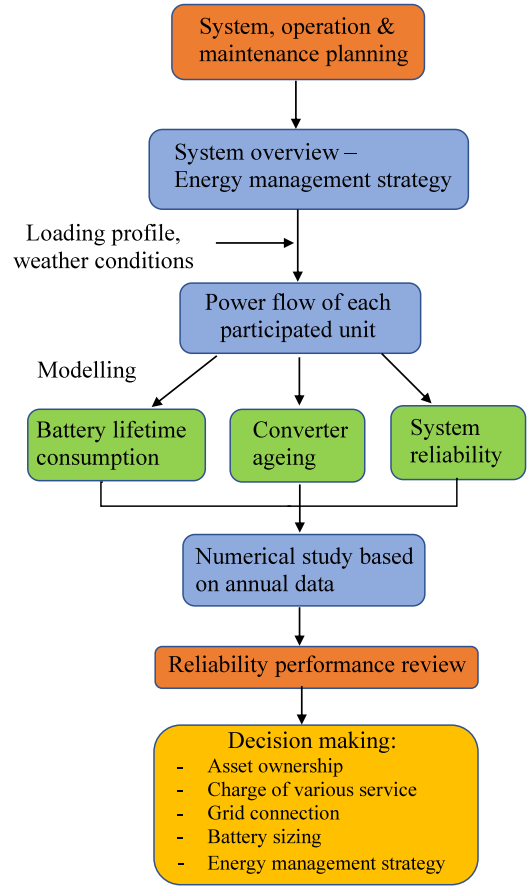


Fig. 1. Process of reliability study for EMS.

2. The energy management strategies

The power generation in the discussed MG is from rooftop PV panels, household batteries or community common batteries and the utility grid. All the power sources and loads are connected in parallel to a common ac bus, as shown in Fig. 2. The topology represents a community composed of three household participants although it can be expanded without losing generality. This section proposes a battery charging & discharging mechanism which protects the battery lifetime. Four EMSs are then proposed and compared under the same system settings, i.e. identical PV/battery models, identical interfacing converter topology and modulation strategies. The difference of these EMSs is the different interaction scheme between parallel-connected power generation units and loads.

2.1. Battery management strategy

The battery management strategy plays a critical role in coordinating different generation units. It protects the battery lifetime by imposing charging and discharging limits. These constraints also dictate the PV power allocation as well as the power exchange with the utility. The charging process for a battery cell can be composed of constant current charging period and constant voltage charging period. The charging rate for a battery source is restricted to the manufacturer's recommended charge/discharge rate (P_{B0}) and the SOC level, following the principles from (1) to (2) [34].

$$P_{ch} = \begin{cases} P_{B0} & \text{if } SOC < SOC_{ref} \\ P_{B0} e^{-\frac{SOC - SOC_{ref}}{\delta SOC / k_{\delta}}} & \text{if } SOC \geq SOC_{ref} \end{cases} \quad (1)$$

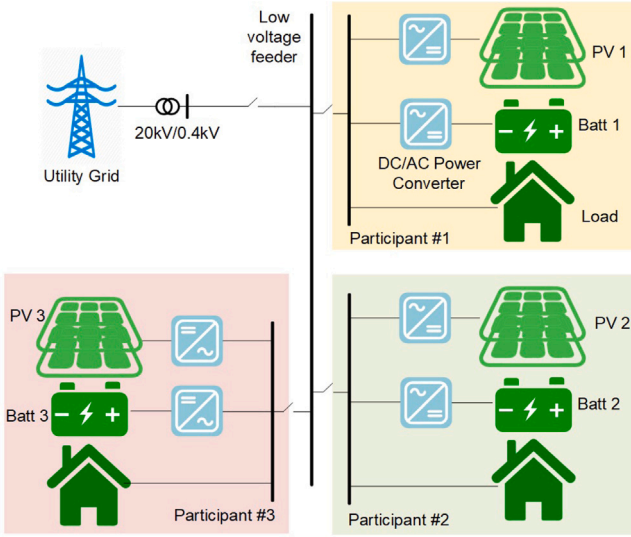


Fig. 2. Structure of a full-power-electronics-based MG with three participants.

where SOC_{ref} is the threshold when constant voltage charging starts; δSOC is the range over which constant voltage charging occurs before the battery is fully charged; k_δ is the charging rate time constant. Meanwhile, the real-time SOC of battery can be estimated by an ampere-hour (Ah) counting method as expressed below [35]:

$$SOC = SOC_0 + \int_0^t \frac{I_{batt}(\tau)}{3600C_{batt}} d\tau \quad (2)$$

where SOC_0 represents the initial SOC, C_{batt} is the capacity of the battery in Ah and I_{batt} is charging current in A. When a battery discharges, the discharge rate is restricted by a maximum value, as specified in (3).

$$P_{B-max} = \begin{cases} P_{B0} & \text{if } SOC > SOC_{low} \\ 0 & \text{if } SOC \leq SOC_{low} \end{cases} \quad (3)$$

where SOC_{low} is the lower threshold of SOC level, below which the battery should stop discharging to prevent depletion.

The battery management strategy is important in the discussion of EMSs. The defined specifications above should be complied with in the following proposed EMSs.

2.2. Energy management strategies

Four EMSs are proposed in this section with the objective of maintaining power balance within the MG. The power flow coordination scheme among PV, battery, local loads and the utility grid, however, varies in each EMS.

2.2.1. Strategy A - independent participants

Strategy A weakens the concept of the community as a whole and encourages individual participants to interact with the main grid directly. The local load is firstly supported by its own PV-battery system and then supported by the main grid if there is power shortage. On the other hand, any redundant PV power generation will be exported to the main grid. PV panels are thus allowed to generate their maximum available power under maximum power point tracking (MPPT) (represented in (4)), which maximizes its utilization. MPPT tracks the maximum available PV power under varying ambient temperature (T_a) and solar irradiance (I_r) [36].

$$P_{pv} = P_{MPPT} \quad (4)$$

Note that the battery is only charged by the local PV power generation and the main grid is only to support the local load (P_L). In

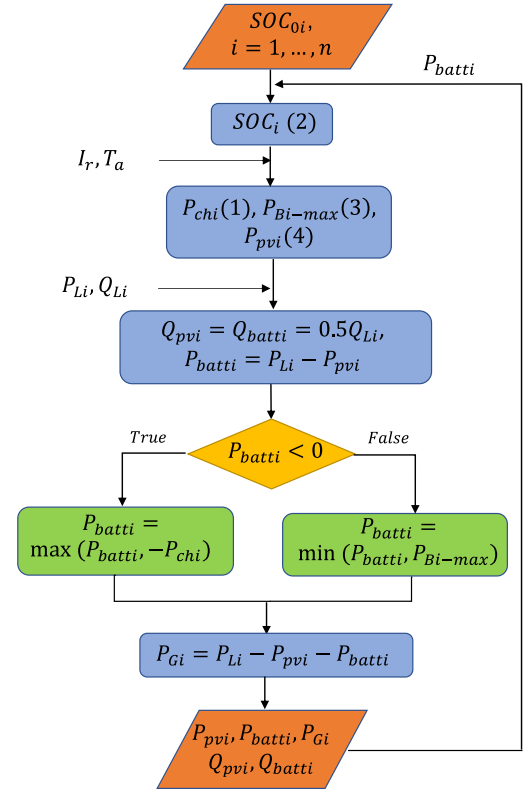


Fig. 3. Participant i operation condition for one cycle under Strategy A with n participants.

the coordination of PV and battery, sufficient PV power generation can support its local demand and standard battery charging P_{ch} . If the PV generation reduces, the charging rate reduces and the battery can even discharge power if PV generation alone cannot support local load. To prevent the battery from becoming too-deeply discharged, the battery discharge rate is restricted by P_{B-max} and any consequent power shortage is met by the main grid. For the sake of simplicity, the reactive power load (Q_L) is assumed to be equally shared by PV and the battery. In a community MG composed of n participants, the power distribution of one participant i for one cycle is presented in a flow chart, as shown in Fig. 3.

2.2.2. Strategy B - community common sources

In Strategy B, the power generation from all PV-battery units is treated as community common power supply. The power consumption of all loads is supported as community common power demand. The community batteries are charged by the PV power generation as a whole and discharge to compensate for power shortage as a result of insufficient PV generation. The power distribution among the connected batteries aims to balance their SOC levels during the course of operation, the scheme of which is explained below.

During the battery charging period, the distribution of total PV generation to parallel-connected batteries is inversely proportional to their real-time SOC levels. During the discharging process, the discharge rate is proportional to the SOC level and total discharging power is to support the common demand. The battery power distribution strategy can be represented by the following equations.

$$P_{batti} \propto \frac{1}{1 - SOC_i}$$

$$\sum_{i=1}^n P_{batti} = \sum_{i=1}^n P_{Li} - \sum_{i=1}^n P_{pvi} \quad (5)$$

$$i = 1, \dots, n$$

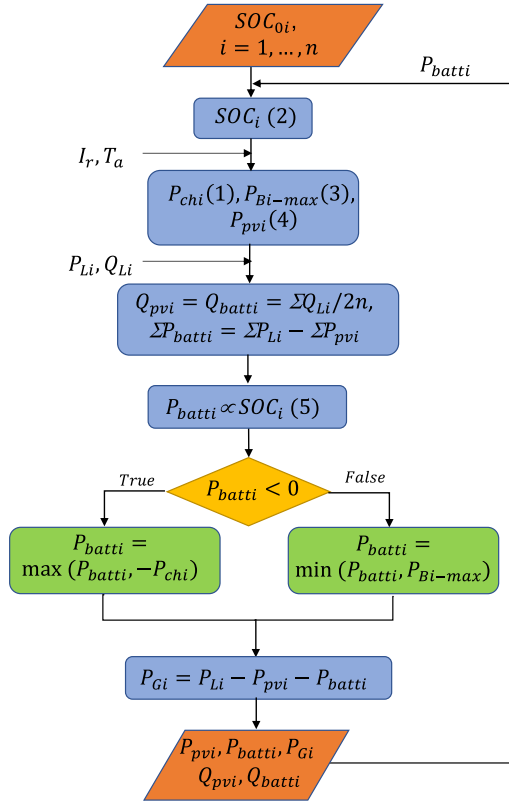


Fig. 4. Participant i operation condition for one cycle under Strategy B with n participants.

where P_{batti} , P_{pvi} and P_{Li} are battery power output, PV power output as well as the local load of Participant i , respectively. Note $P_{batti} > 0$ when discharging and $P_{batti} < 0$ when being charged. The power distribution under Strategy B can be represented as in Fig. 4.

2.2.3. Strategy C - inter-unit PV power transmission

Strategy C tries to utilize the PV generation within the community before exporting to the utility grid. If a participant's local PV generation is sufficient to support its own load and maximum battery charging rate, the redundant PV power can be distributed to its neighbours who require power inputs. Every participant can generate a power request if its available PV-battery power supply cannot meet its local power demand. If all loads are fully supported by the community sources, the redundant PV generation is exported to the utility grid. In the case when community power generation is not enough to support the community load demand, the import from the utility grid will meet the power requests.

The power transmission between participants only occurs when two criterion i.&ii. are met simultaneously:

- i. Redundant PV power generation appears in one participant;
- ii. A power request from the community is received.

where the requested power (P_{reqi}) of Participant i is determined by (6) and the redundant power (P_{exti}) generated from Participant i can be determined by (7).

$$P_{reqi} = \max(P_{Li} - P_{pvi} - P_{batti}, 0) \quad (6)$$

$$P_{exti} = \max(P_{pvi} - P_{Li} - P_{batti}, 0) \quad (7)$$

Correspondingly, the system condition for one cycle under Strategy C is shown in Fig. 5.

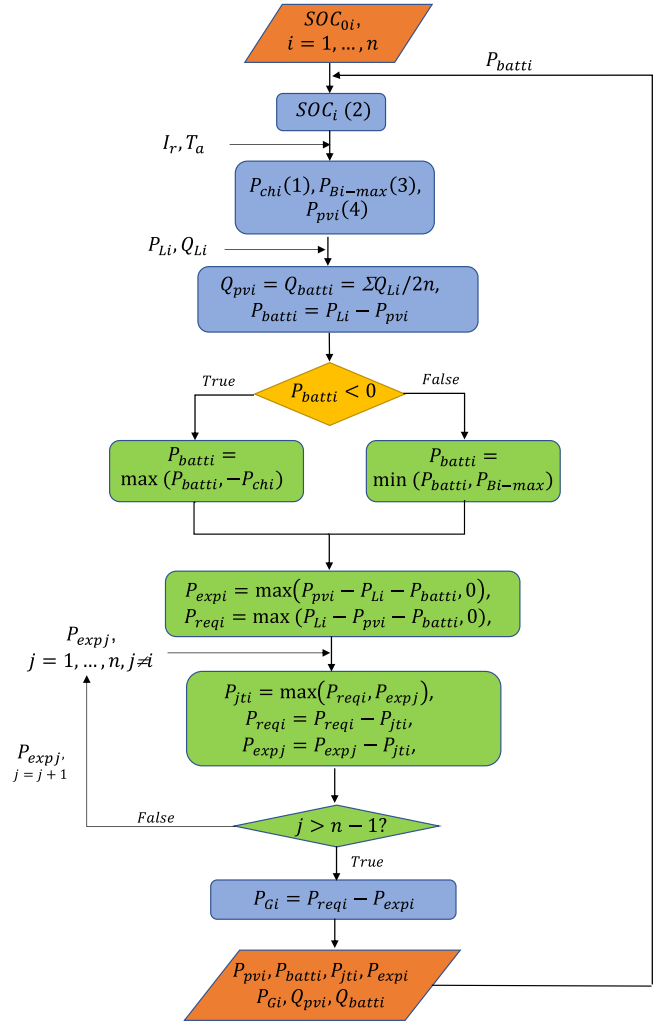


Fig. 5. Participant i operation condition for one cycle under Strategy C with n participants.

2.2.4. Strategy D - critical load

Similar to Strategy C, the community PV generation in Strategy D also has the responsibility in supporting community loads rather than exporting to the utility. In addition, it takes into account the critical level of load demand. If critical loads are identified in a participant, they are prioritized in power distribution. Prioritized loads are firstly supported by its local PV-battery generation, and can also be supported by neighbours' PV panels and batteries. Neighbours' batteries are to support power requests as long as their discharge rates are within the constraint P_{B-max} .

The power transmission between participants occurs under the same criterion i.&ii. However, the exportable power from participant i increases for prioritized loads, which are represented by $P_{ext'i}$.

$$P_{ext'i} = \max(P_{pvi} - P_{Li} + P_{Bi-max}, 0) \quad (8)$$

The power distribution algorithm under Strategy D is shown in Fig. 6. In the flowchart, $P_{ext'i}$ is the exportable power of Participant i to support prioritized loads; P_{exti} is the exportable power of Participant i to support normal loads and P_{reqi} is its power request.

A summary of the proposed four strategies is shown in Table 1, where the main differences are listed.

3. Reliability analysis

In this section, reliability analysis in PV-battery-based MGs will be discussed from different perspectives.

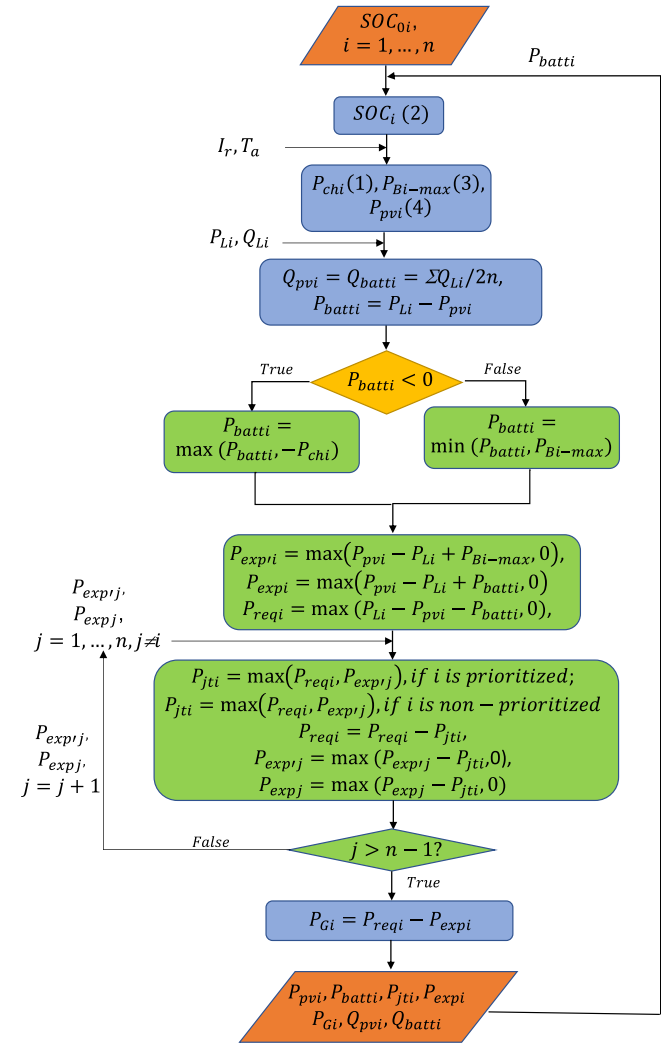


Fig. 6. Participant i operation condition for one cycle under Strategy D with n participants.

Table 1
Features of unit interaction and battery SOC under the proposed EMSs.

EMSs	Utility support	Mutual PV support	Mutual battery support	Balanced SOC
A	✓	×	×	×
B	✓	✓	✓	✓
C	✓	✓	×	×
D	✓	✓	✓	×

3.1. Battery lifetime model

Since the life cycle of batteries in a hybrid power system plays a significant role in system expenses, battery lifetime modelling is a very important aspect. In a project shown in [7], the major stress factors on battery damage were identified: discharge rate, time at low state of charge, Ah throughput, charge factor, time between full charge, partial cycling and temperature. In this paper, the common cycle counting method is used to estimate the battery lifetime, by focusing on current flow and SOC of the battery. The number of cycles to failure varies with the depth of discharge. As a result, the battery damage during a time period needs to be calculated by appropriate summation of all individual conditions.

The specifications of cycle to failure of a battery are usually specified by the manufacturer. For a Trojan deep-cycle gel lead-acid battery,

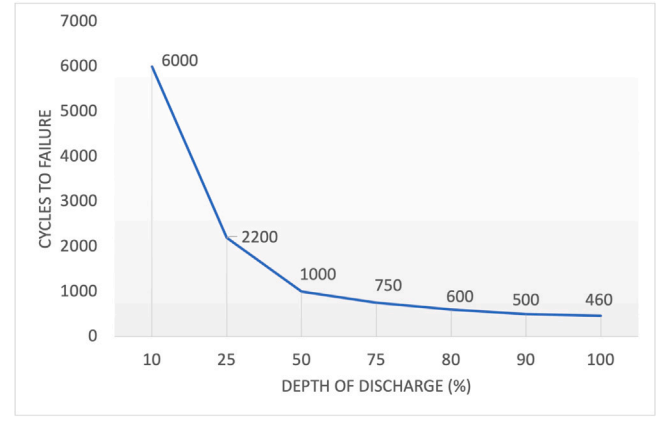


Fig. 7. Cycles to failure at different depth of discharge (DOD) of a lead-acid battery.

the number of cycles to failure N_{ctf} at different depth of discharge (DoD) can be seen in Fig. 7 (orange marker) [37]. Polynomial regression can be used to simulate the correlation between the two variables. Using Matlab Polyfit function, the data shown in Fig. 7 can be modelled with the expression below:

$$N_{ctf} = 59600 \cdot DoD^4 - 160640 \cdot DoD^3 + 156030 \cdot DoD^2 - 65670 \cdot DoD + 11160 \quad (9)$$

This fourth-order polynomial regression has a coefficient of determination $R^2 = 0.9997$. The closer R^2 to 1, the better the model predicts the actual value. This model is plotted in Fig. 7 and it can be seen that the predicted value matches with the actual value closely.

During operation, the battery can experience different levels of discharge in each individual cycle. Each DoD value corresponds to a specific N_{ctf} value and the loss of battery lifetime during the operating period is defined as given below [38].

$$LOL_{batt} = \sum_{DoD=0.01}^{DoD=1} \frac{N_{cyc}(DoD)}{N_{ctf}(DoD)} \quad (10)$$

where $N_{cyc}(DoD)$ is the number of full cycles at the specific depth-of-discharge DoD. The end of life of the battery is reached when $LOL_{batt} = 1$. In order to count N_{cyc} for a time period, the rain-flow-counting method can be used.

3.2. Power electronics reliability

Given that DC-AC power converter is commonly used in DG interfacing, its reliability modelling is analysed here. Similar to the battery reliability model, converter reliability can also be assessed by its lifetime consumption, which can be determined by converter lifetime modelling and thermal performance monitoring. Because the converter failures are dominated by the most vulnerable components, semiconductor devices normally become the focus of reliability assessment [29]. The junction temperature swing (ΔT_j) on semiconductors is critical to their lifetime [30]. In power converters, the employed semiconductor devices are insulated-gate bipolar transistor (IGBT) and diode, whose lifetime model can be represented as given below [39].

$$N = A \cdot \Delta T_j^\alpha \cdot \exp\left(\frac{\beta}{T_{jm} + 273.15}\right) t_{on}^\gamma \quad (11)$$

where N is number of cycles to failure; T_{jm} and ΔT_j represent minimum junction temperature and temperature swing of the cycle, respectively; t_{on} is the heating time; A , α , β , and γ are constants obtained from long-term lifetime tests. The lifetime consumption after an operating period can then be calculated based on its thermal cycling:

$$D = \sum_i \frac{n_i}{N_i} \quad (12)$$

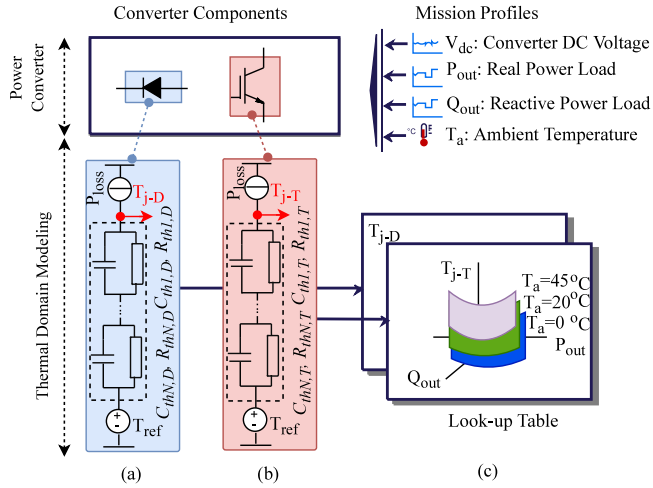


Fig. 8. The procedure of electro-thermal mapping in the power converter: (a) Diode (b) IGBT (c) Look-up Table.

where D is the thermal damage of the device under n_t thermal cycles during the operation period of t . N_t is the number of cycles to failure derived from (11) under the corresponding thermal cycles with T_{jm} , ΔT_j , and t_{on} .

Since IGBT and diode experience different thermal profiles, the thermal damage on each device needs to be calculated separately. The total thermal damage on a converter can then be represented by:

$$D_{converter} = \max\{D_{gT}^{(T)}, D_{gD}^{(D)}\}, \quad (13)$$

where $g_T \in \{1, \dots, M^{(T)}\}$, $g_D \in \{1, \dots, M^{(D)}\}$ and $M^{(T)}$, $M^{(D)}$ are numbers of IGBT and diodes in each converter; $D_{gT}^{(T)}$ and $D_{gD}^{(D)}$ represent the thermal damage on a single IGBT and diode respectively in the discussed converter.

It can be seen that the thermal performance of a converter is critical in its reliability assessment. It can be attained by directly measuring junction temperature [40] or by electro-thermal mapping estimation [31]. Considering the requirement of costly temperature sensors in direct measuring method, the electro-thermal mapping method is adopted here, whose procedure is described in Fig. 8 [28]. The thermal model of IGBT and diode should first be established, which includes parameters for thermal impedances, turn on-off switching energy, and V-I curves when conducting. Thermal impedances will increase the junction temperature T_j when dissipating power losses. The steady-state junction temperature is mainly dependent on the thermal resistance R_{th} while its dynamic behaviour is mostly dependent on thermal capacitance C_{th} . The operating conditions that will affect the junction temperature are: converter power flow, ambient temperature and DC link voltage. The impact of DC link voltage is ignored here for the sake of simplicity, while it can be included in future research, as it will have influence on the losses. The thermal modelling helps to develop a look-up table for T_j monitoring. When the system in operation, the T_j profiles of every device can be obtained based on real-time measured power flow and T_j look up table. Ultimately, the converter thermal damage profile can be created based on (11) to (13).

To identify all the thermal cycles during an operating period, rain-flow-counting method can also be used to group the cycles with the same specifications (T_{jm} , ΔT_j , t_{on}) [41]. The thermal damage on a component is the sum of thermal damage from all thermal cycles according to (12).

3.3. Reliability of power system

The power system reliability is measured as its ability to supply the loads. This is usually assessed by adequacy indices like Loss Of Load

Table 2

Specifications of PV and Battery in numerical analysis.

Parameters	Participant1	Participant2	Participant3
PV	3 kW	3.6 kW	3 kW
Battery	20 Ah	24 Ah	20 Ah
P_{B0}	3 kW	3.6 kW	3 kW
V_{Batt}	150 V		
SOC_0	0%		
f_{sw} (Converter)	10 kHz		
IGBT (Converter)	IGBT20N60H3		
Diode (Converter)	IDV15E65D2		

Expectation (LOLE) and Expected Energy Not Supplied (EENS) [42]. EENS is the amount of load that is not supplied due to power system outage during the course of operation. In this paper, it is used for evaluating the MG power system reliability, which is obtained by:

$$EENS = \sum_{i=1}^n P_i \cdot E_i \quad (14)$$

where P_i is the probability of power outage during event i , and E_i is the energy not supplied in this event. The procedure of availability prediction is discussed in [42]. A power system with lower EENS is more reliable as the amount of un-supplied load is lower.

4. Power and energy flow

Simulations and numerical analysis are conducted based on the introduced EMSs in the community MG as shown in Fig. 2. The simulated MG is composed of three household participants connected in parallel. The power supply in every household is from a PV unit plus a battery unit. The system specifications are summarized in Table 2. In addition, the parameters of battery management are set as: $SOC_{low} = 20\%$, $SOC_{ref} = 80\%$, $\delta SOC = 10\%$ and $k_\delta = 10$. It is reasonable to assume that every household within the community experience similar weather conditions due to geographic proximity. The annual weather conditions of the studied community are shown in Fig. 9(a), (b). Since PV panels operate under MPPT, PV power output is dependent on the PV panel rating and the local weather conditions (i.e. I_r , T_a). The PV rating is designed in a way that the total annual PV energy largely equals annual household energy consumption.

It is unlikely for different households to experience the same loading profile. The detailed annual mission profiles for each household are shown in Fig. 9(d) to (f) and the load is assumed to have a power factor of $pf = 0.9$. Participant1 has an office-like load pattern. Participant2 and Participant3 has a household-like load pattern but at different consumption levels. The PV rating in Participant 2 is higher due to its higher annual energy consumption. Meanwhile, PV power generation of Participant 1 and Participant 3 are identical due to their same PV ratings (Fig. 9(c)). Note that the local data are collected on one-minute-basis. In the following, the impact of different EMSs on the power flow is presented.

4.1. Strategy A

The annual power sharing performance based on the proposed Strategy A is shown in Fig. 10. The battery is charged for most of the days when I_r is high and discharges at night to support the load demand. Because every participant is independent, they have their unique profiles of battery power flow (Fig. 10(a)) and SOC level (Fig. 10(b)). The interaction with the utility grid is also shown in Fig. 10(c). The positive values correspond to power injected into the community MG while negative values correspond to power exported out of the community MG.

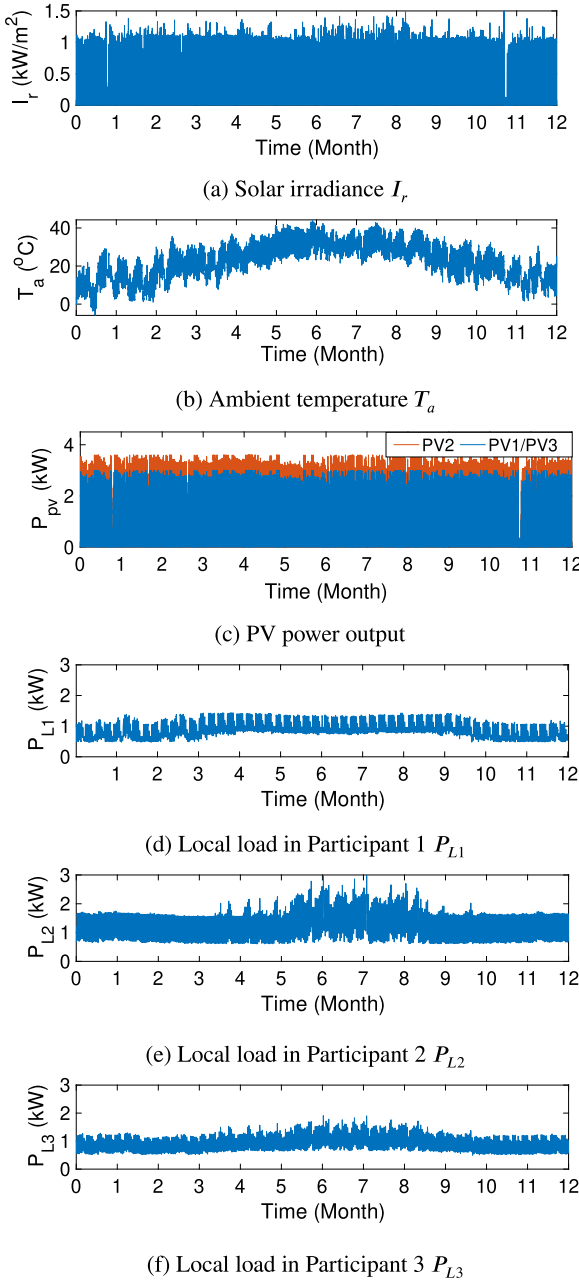


Fig. 9. Annual mission profiles: weather conditions, PV generation and local loads of each participants in the microgrid.

4.2. Strategy B

The annual power sharing performance based on the Strategy B is shown in Fig. 11. From Fig. 11(a), we can see that the battery in Participant 2 has less power flow compared to Fig. 10(a). This is because all batteries share the same target, which is to equalize SOC levels while maintaining power balance. The reduction of power flow through Batt 2 is compensated by Batt 1&3. The grid interaction takes place when there is power imbalance after reaching the battery charging/discharging limits. Compared to Strategy A, participants have a complicated interaction with the grid due to the aim of balancing SOC.

4.3. Strategy C

When a participant is allowed to transfer PV power to its neighbours, the interaction of the community with the utility grid is supposed

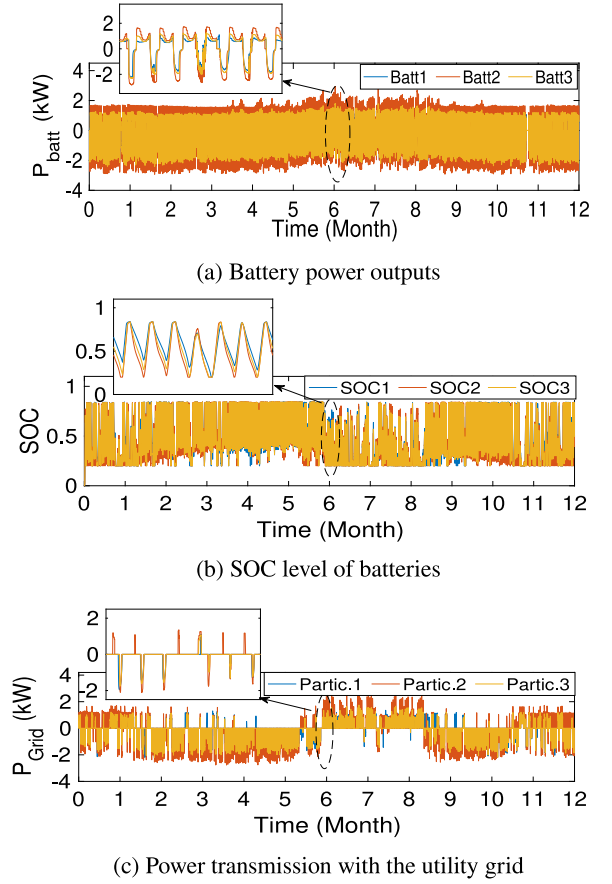


Fig. 10. Annual MG performance of battery power outputs, SOC level and injected power from the utility grid under Strategy A.

to reduce. Some redundant PV power will flow to support neighbours load before exported to the utility. Conversely, the generated local power requests will be met by neighbours PV power before sent out to the utility. The simulation results based on the proposed MG settings are shown in Fig. 12. It is found that these power distribution profiles are the same as Strategy A. This finding is also proved by zero inter-unit transmission record during the simulation period. This phenomenon can be explained by the fact that there is no redundant PV power available within the system when a power request is received. This is usually the case when the installed PV panels are in geographic proximity and the PV rating is related with the energy consumption. Power requests are likely to be generated simultaneously across all the participants and no redundant PV power is available at the same time. However, if the installed PV in one participant has a higher rating, inter-unit power transmission may be observed under Strategy C.

4.4. Strategy D

Since Strategy D allows batteries to support neighbourhood loads, the chance of inter-unit power transmission increases. As a result, the battery operation conditions and grid interaction performance will be different from Strategy C. In the simulation, the load of Participant 1 is classified as the high-priority load and batteries in Participant 2&3 are thus required to support Participant 1. The power distribution results are shown in Fig. 13(a)–(c) and the inter-unit transmission is shown in Fig. 13(d). It can be seen that Participant 2&3 transfer power to Participant 1 from time to time, while no transmission occurred for normal loads.

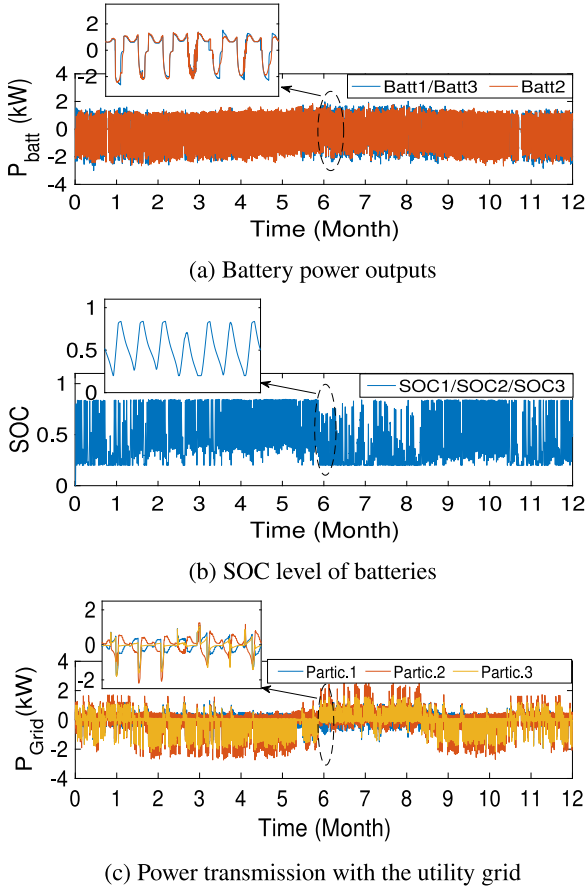


Fig. 11. Annual MG performance of battery power outputs, SOC level and injected power from the utility grid under Strategy B.

5. Reliability analysis and discussions

In this section, the MG reliability will be discussed from different perspectives: battery lifetime consumption, converter thermal damage and system reliability. The evaluation of the proposed EMSs will be based on the simulation results obtained in the last section.

5.1. Battery lifetime consumption

The operating condition of the batteries during one year operation is recorded in their SOC profiles. The number of cycles across the operating period at a specific DoD can be calculated based on a rainflow algorithm. Fig. 14 has shown an example of cycle counting for the battery in Participant 1 under Strategy A.

After obtaining the number of cycles, the damage to the battery, which is mainly due to discharge depth, can be analysed. The lifetime consumption analysis is shown in Fig. 15. According to the figure, Strategy A and Strategy C experience the same power flow, which leads to the same lifetime consumption on batteries. According to the results, Strategy D also causes similar battery damage as Strategy A due to the little power transmission between participants. The major difference can be found in the performance under Strategy B, as shown in Fig. 15(b). The battery in Participant 2 suffers 14% less damage than other participants. In comparison, it suffers 14% more damage under Strategy A.

It can be concluded that the contribution of energy consumption level on battery lifetime consumption can be altered by the EMS. Although Participant 2 consumes more energy, its battery unit will suffer less damage under a different EMS, i.e. Strategy B. This can

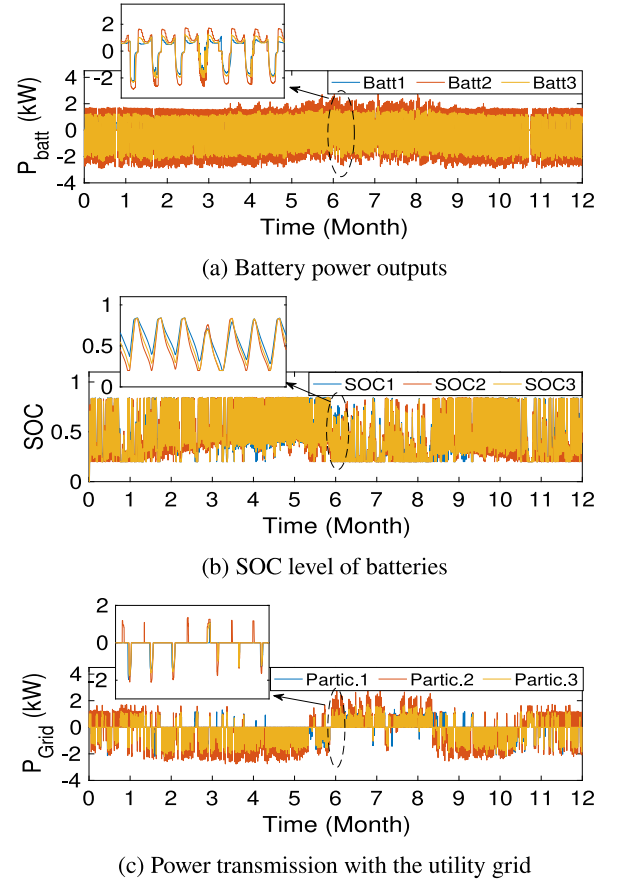


Fig. 12. Annual MG performance of battery power outputs, SOC level and injected power from the utility grid under Strategy C.

provide a new perspective in system design and maintenance planning. Moreover, the asset ownership shall also be considered in decision-making. Strategy B is more recommended to utility ownership rather than the private ownership, since Participant 2 enjoys longer battery service time with the sacrifice of neighbour batteries.

5.2. Converter reliability

Because different EMSs lead to different power flow through the interfacing converters, the accumulated thermal damage on the converters also varies. For a full-bridge three phase DC/AC converter, its thermal damage can be estimated based on the lifetime model discussed in Section 3.2. According to [39], the parameters of (11) are chosen as follows: $A = 9.34 \times 10^4$, $\alpha = -4.416$, $\beta = 1290$, and $\gamma = -0.3$. PLECS is employed to create the electro-thermal look-up table based mapping on the specified semiconductor type. The rain flow counting described in [41] is adopted here to estimate the converter damage based on the annual mission profiles.

The converter annual thermal damage based on the simulated power flow is shown in Fig. 16. It can be seen that the converter damage behaves similarly when the participants are relatively independent (Strategy A&C&D), according to Fig. 16(a), (c) and (d). Both PV2 and Batt2 converters suffer from more damage than their neighbouring counterparts, due to the higher energy consumption in Participant 2. Meanwhile, the thermal damage on the battery converter is 37% higher than PV converter in Participant 2.

However, Strategy B (Fig. 16(b)) causes dramatic damage reduction on the battery converter in Participant 2. It drops to the same level as other battery converters. It now suffers less damage than the PV

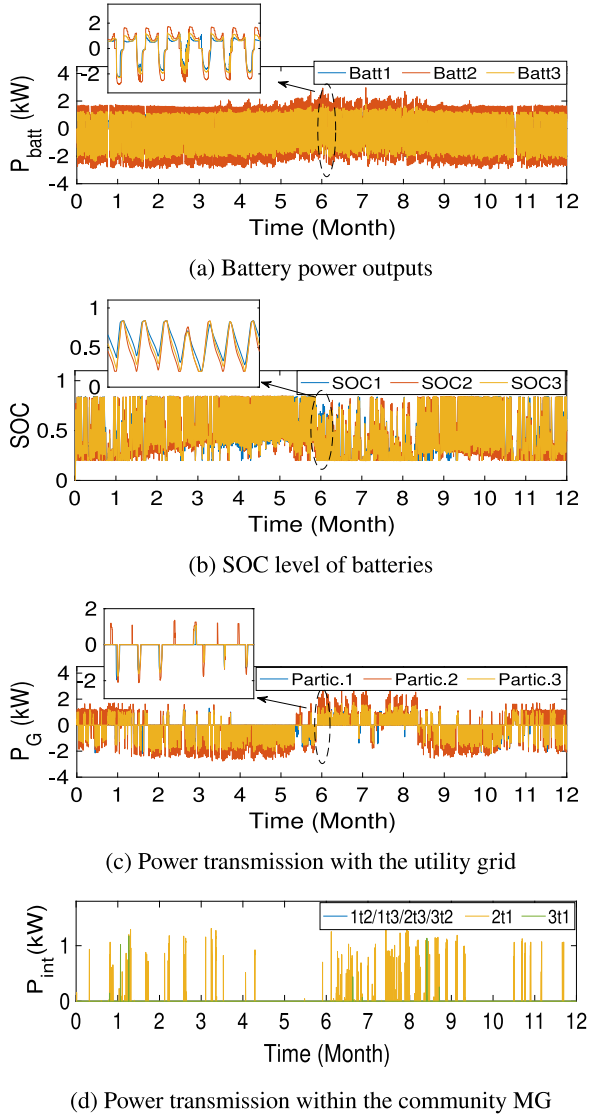


Fig. 13. Annual MG performance of battery power outputs, SOC level and injected power from the utility grid under Strategy D.

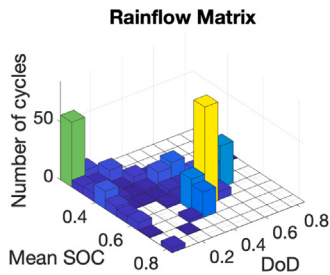


Fig. 14. Battery discharge cycles counting of DoD levels after one year operation in Participant 1 under Strategy A for the mission profiles given in 9.

converter by 71%. This reduction can be explained by a closer look on the battery power distribution.

A typical weekly power flow under Strategy B is shown in Fig. 17. By focusing on a typical day in June (circled), the output power of a battery under strategy A varies among different participants, where Participant 2 discharges more power due to the higher power demand and higher P_{B-max} . The corresponding SOC level drops to the minimum threshold quickly and then stays idle. By contrast, the battery

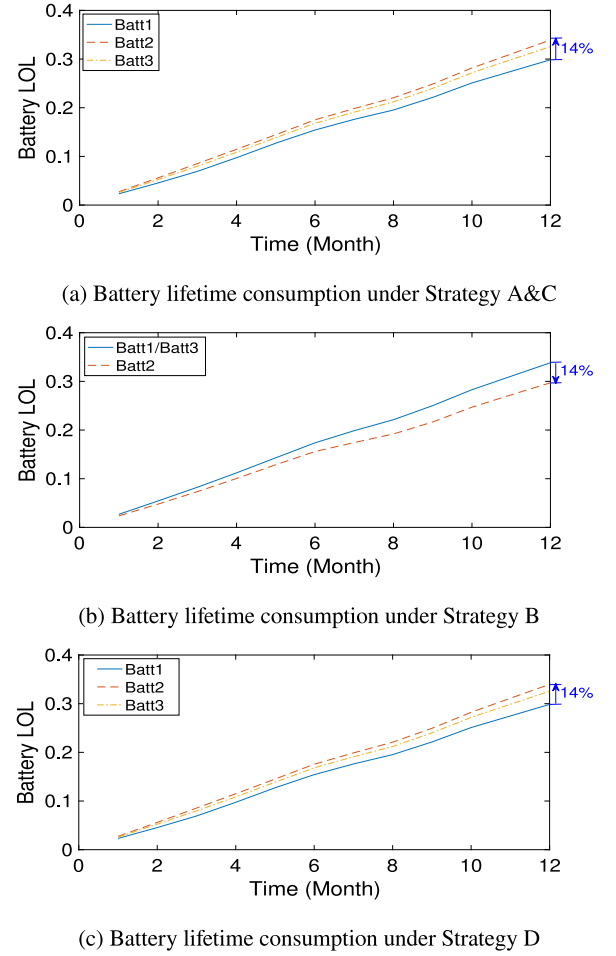


Fig. 15. Battery lifetime consumption measured by LOL index during one-year operation for the mission profiles given in 9.

in Participant 1 discharges at a relatively constant rate until fully discharged. This difference causes the variant thermal cycles and in turn thermal damages on the battery converters as shown in Fig. 16(a). As for Strategy B, all batteries within the community share the same duty. The battery power flow is maintained balanced and the SOC levels are kept as identical as possible. In the circled period, Participant 1&3 increases their power discharge to support the load in Participant 2. As a consequence, the three batteries suffer similar thermal damages.

It is thus clear that the converter service time depends on the local load level as well as the adopted EMS. At participant level, the PV converter is to be replaced later than the battery converter in Participant 2 under Strategy A&C&D, while to be replaced earlier under Strategy B. At system level, the converter (e.g. Batt2 converter) ageing can slow down under a different EMS (Strategy B). In summary, the maintenance planning cannot effectively be scheduled without considering the adopted EMS. Meanwhile, the electricity bills merely based on power metering cannot reflect the real energy cost, where the converter damage also plays an important role.

5.3. Power system reliability analysis

Power system reliability is assessed based on the incidence associated with the power outage, i.e. Expected Energy Not Supplied (EENS) [43,44]. The impacts of utility grid forced outage rate (FOR) and battery FOR are both analysed in this section. The PV and grid failure rates are controlled variables when investigating battery failures. According to [45], the controlled variable is chosen as 0.05 of FOR.

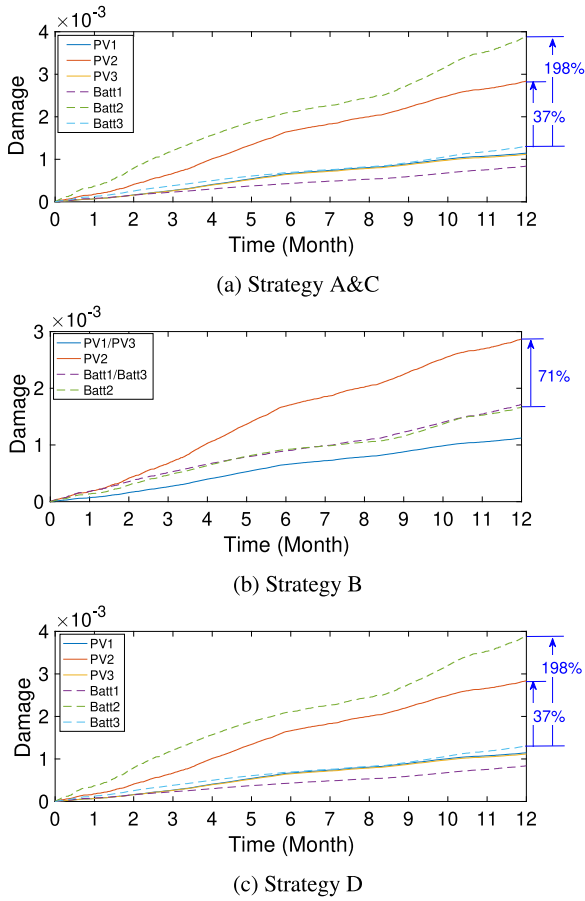


Fig. 16. The annual thermal damage of converters during one-year operation for the mission profiles given in 9.

5.3.1. Outage of utility grid

Because the utility grid provides backup power to the community MG, its reliability level will affect the EENS suffered in the community MG. Different annual outage hours of the grid are assumed and the corresponding EENS are shown in Fig. 18. It is obvious that as the grid failure rate increases, the annual load loss increases. Although the MG has batteries as energy storage, it still suffers tremendously from load loss in islanded mode.

In islanded mode, Strategy B causes more load loss in all the participants because the power sources within the community exchange power with the grid more often than other strategies. This coincides with the finding in Fig. 11(c). It can also be seen that under Strategy D, Participant 1 has a lower rate of change of EENS due to the extra support from neighbours' batteries. Note that its overall higher EENS value under Strategy D can also be attributed to its reliance on batteries, which has a FOR rate of 0.05 in this simulation.

In summary, Strategy B is not recommended for a MG connected to a weak grid. Meanwhile, if there is critical load in the MG, an advanced energy storage system is suggested, which can reduce the impact of grid failure on power reliability.

5.3.2. Outage of batteries

Since battery lifetime consumption behaves differently under different EMSs, it further affects the power reliability of the system as a whole. Different outage rates of the batteries are assumed and the corresponding EENS is shown in Fig. 19. While the load loss increases consistently as battery failure rate rises for Strategy A&B, Strategy C has a (up to 220%) higher rate of change of EENS. In addition, battery failure has a higher impact on critical loads, i.e. Participant 1,

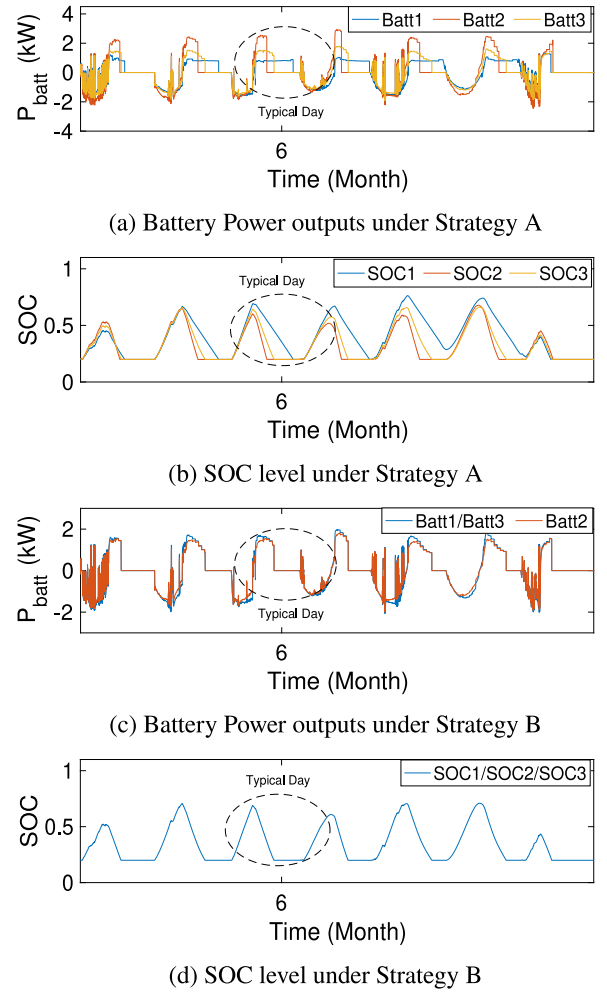


Fig. 17. Weekly MG performance of battery power outputs and SOC level from the utility grid under Strategy A&B.

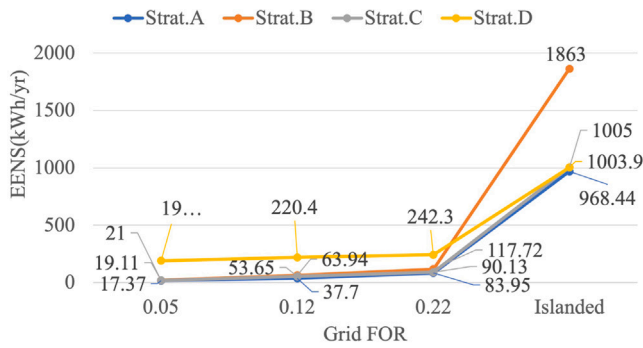
Table 3
Reliability performance review of the proposed four EMSs.

EMSs	Battery lifetime consumption	Converter ageing	System reliability
A	Correlated with energy consumption level		–
B	Balanced across network; Battery units can save >50% lifetime in large energy consumers		Up to 92% more load loss at a higher utility grid failure rate
C	Correlated with energy consumption level		Up to 220% higher increase rate of load loss at a higher battery failure rate
D	Correlated with energy consumption level		Up to 7 times higher impact on critical load supply

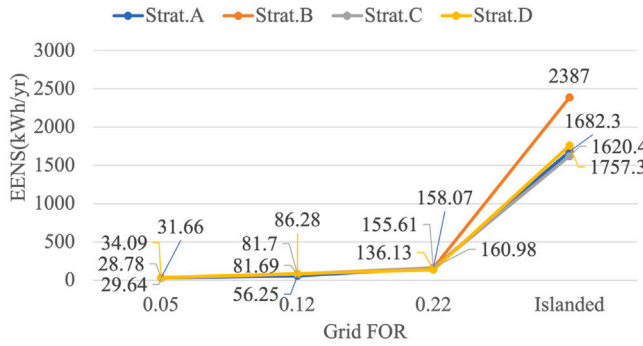
under Strategy D. These phenomena can remind the participant that the system has more reliance on batteries under Strategy C&D but the effect of Strategy C becomes more obvious under a higher failure rate.

6. Conclusions

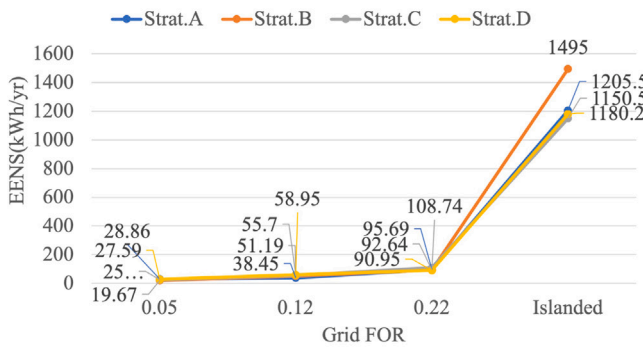
This paper has analysed the reliability performance of a community MG from multiple perspectives. The battery lifetime consumption and converter thermal damage are used as the criterion on device level assessment. Meanwhile, the EENS indicates the system level reliability.



(a) Participant 1



(b) Participant 2



(c) Participant 3

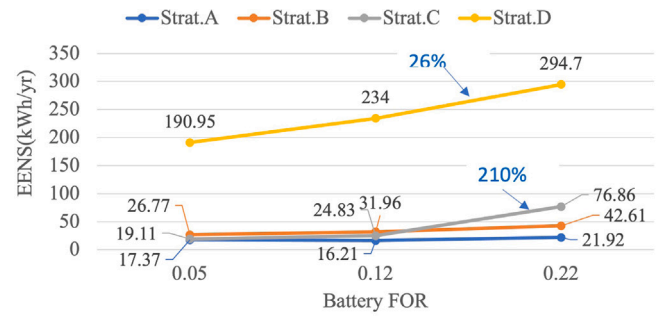
Fig. 18. Obtained system reliability with the annual EENS for four EMSs under varying utility grid forced outage rate (FOR) from 0.05 to fully islanded.

The proposed four different EMSs are assessed from these three perspectives and their impacts are thoroughly analysed and compared, which can be summarized in Table 3.

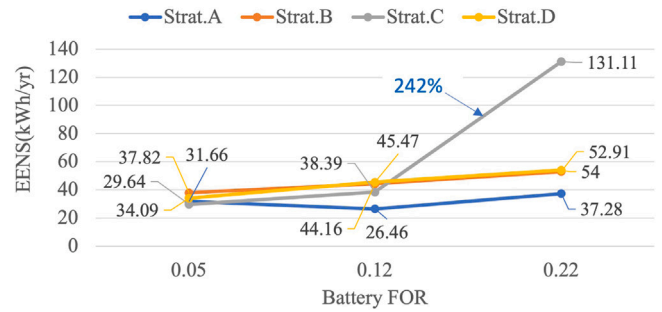
It is found that the EMS can alter device lifetime consumption even under the same level of load demand. Different EMSs also affect the power supply reliability level under contingencies. This paper provides a new perspective for MG management and maintenance planning. Moreover, it suggests to the energy market operator that the device consumption level and power supply reliability will play an important role as the grid integrates more DG. Future studies can integrate advanced optimization algorithms in the design of EMS. It can also be developed into an on-line reliability assessment strategy which adjusts the EMS in real-time to achieve higher cost efficiency.

Ethics statement

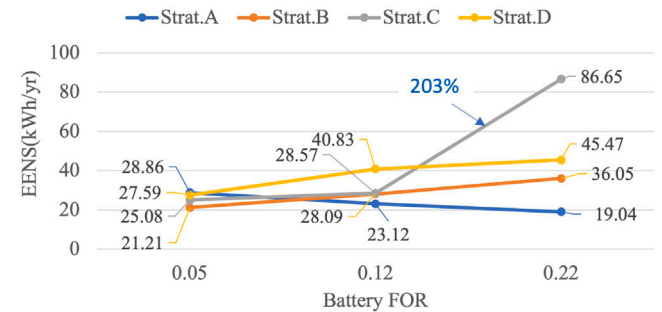
The authors hereby confirms that the submitted work is not related to the animal and/or human subjects.



(a) Participant 1



(b) Participant 2



(c) Participant 3

Fig. 19. Obtained system reliability with the annual EENS for four EMSs under varying battery forced outage rate (FOR) from 0.05 to 0.22.

References

- [1] F. Blaabjerg, Y. Yang, D. Yang, X. Wang, Distributed power-generation systems and protection, *Proc. IEEE* 105 (2017) 1311–1331.
- [2] IEA (2019), "world energy outlook 2019", IEA, Paris, 2019, <https://www.iea.org/reports/world-energy-outlook-2019>.
- [3] R.H. Lasseter, Extended CERTS microgrid, in: 2008 IEEE Power and Energy Society General Meeting - Conversion and Delivery of Electrical Energy in the 21st Century, 2008, pp. 1–5.
- [4] S. Peyghami, P. Palensky, F. Blaabjerg, An overview on the reliability of modern power electronic based power systems, *IEEE Open J. Power Electron.* 1 (2020) 34–50.
- [5] S. Abu-Sharkh, R.J. Arnold, J. Kohler, R. Li, T. Markvart, J.N. Ross, K. Steemers, P. Wilson, R. Yao, Can microgrids make a major contribution to UK energy supply? *Renew. Sustain. Energy Rev.* 10 (2006) 78–127.
- [6] H. Rahimi-Eichi, U. Ojha, F. Baronti, M. Chow, Battery management system: An overview of its application in the smart grid and electric vehicles, *IEEE Ind. Electron. Mag.* 7 (2013) 4–16.
- [7] H. Bindner, T. Cronin, P. Lundsager, J.F. Manwell, U. Abdulwahid, I. Baring-Gould, Lifetime modelling of lead acid batteries, Vol. 12, 2005.
- [8] S.A. Arefifar, Y.A.-I. Mohamed, T.H.M. EL-Fouly, Optimum microgrid design for enhancing reliability and supply-security, *IEEE Trans. Smart Grid* 4 (2013) 1567–1575.

- [9] Y. Zhang, N. Gatsis, G.B. Giannakis, Robust energy management for microgrids with high-penetration renewables, *IEEE Trans. Sustain. Energy* 4 (4) (2013) 944–953.
- [10] H. Farzin, M. Fotuhi-Firuzabad, M. Moeini-Aghtaie, Stochastic energy management of microgrids during unscheduled islanding period, *IEEE Trans. Ind. Inf.* 13 (2017) 1079–1087.
- [11] C. Battistelli, Y.P. Agalgaonkar, B.C. Pal, Probabilistic dispatch of remote hybrid microgrids including battery storage and load management, *IEEE Trans. Smart Grid* 8 (2017) 1305–1317.
- [12] M. Marzband, S.S. Ghazimirsaeid, H. Uppal, T. Fernando, A real-time evaluation of energy management systems for smart hybrid home microgrids, *Electr. Power Syst. Res.* 143 (2017) 624–633.
- [13] J. Soares, M.A.G. Fotouhi, N. Borges, Z. Vale, A stochastic model for energy resources management considering demand response in smart grids, *Electr. Power Syst. Res.* 143 (2017) 599–610.
- [14] T.A. Youssef, M. El Hariri, A.T. Elsayed, O.A. Mohammed, A DDS-based energy management framework for small microgrid operation and control, *IEEE Trans. Ind. Inf.* 14 (3) (2017) 958–968.
- [15] N.T. Mbungu, R.C. Bansal, R. Naidoo, V. Miranda, M. Bipath, An optimal energy management system for a commercial building with renewable energy generation under real-time electricity prices, *Sustainable Cities Soc.* 41 (2018) 392–404.
- [16] K. Kusakana, Optimal peer-to-peer energy management between grid-connected prosumers with battery storage and photovoltaic systems, *J. Energy Storage* 32 (2020) 101717.
- [17] M. Panwar, S. Suryanarayanan, R. Hovsapian, A multi-criteria decision analysis-based approach for dispatch of electric microgrids, *Int. J. Electr. Power Energy Syst.* 88 (2017) 99–107.
- [18] V.S. Tabar, M.A. Jirdehi, R. Hemmati, Sustainable planning of hybrid microgrid towards minimizing environmental pollution, operational cost and frequency fluctuations, *J. Cleaner Prod.* 203 (2018) 1187–1200.
- [19] Z. Jun, L. Junfeng, W. Jie, H. Ngan, A multi-agent solution to energy management in hybrid renewable energy generation system, *Renew. Energy* 36 (5) (2011) 1352–1363.
- [20] M.A. Jirdehi, V.S. Tabar, R. Hemmati, P. Siano, Multi objective stochastic microgrid scheduling incorporating dynamic voltage restorer, *Int. J. Electr. Power Energy Syst.* 93 (2017) 316–327.
- [21] D.H. Tungadio, R.C. Bansal, M.W. Siti, N.T. Mbungu, Predictive active power control of two interconnected microgrids, *Technol. Economics Smart Grids Sustain. Energy* 3 (1) (2018) 1–15.
- [22] N. Gholizadeh, M. Abedi, H. Nafisi, M. Marzband, A. Loni, G.A. Putrus, Fair-optimal bilevel transactive energy management for community of microgrids, *IEEE Syst. J.* (2021).
- [23] H. Haddadian, R. Noroozian, Multi-microgrids approach for design and operation of future distribution networks based on novel technical indices, *Appl. Energy* 185 (2017) 650–663.
- [24] N.T. Mbungu, R.C. Bansal, R.M. Naidoo, M. Bettayeb, M.W. Siti, M. Bipath, A dynamic energy management system using smart metering, *Appl. Energy* 280 (2020) 115990.
- [25] A. Bani-Ahmed, M. Rashidi, A. Nasiri, H. Hosseini, Reliability analysis of a decentralized microgrid control architecture, *IEEE Trans. Smart Grid* 10 (2019) 3910–3918.
- [26] X. Guo, L. Wang, Y. Zhao, G. Wang, G. Liu, Q. Zhong, Reliability-oriented selection for grid-connected converters: A low voltage direct current microgrid case study, *IEEE Access* 8 (2020) 205836–205847.
- [27] W. Zhong, L. Wang, Z. Liu, S. Hou, Reliability evaluation and improvement of islanded microgrid considering operation failures of power electronic equipment, *J. Mod. Power Syst. Clean Energy* 8 (2020) 111–123.
- [28] J. Jiang, S. Peyghami, C. Coates, F. Blaabjerg, A decentralized reliability-enhanced power sharing strategy for PV-based microgrids, *IEEE Trans. Power Electron.* 36 (2021) 7281–7293.
- [29] H. Wang, M. Liserre, F. Blaabjerg, P.d.P. Rimmen, J.B. Jacobsen, T. Kvisgaard, J. Landkildehus, Transitioning to physics-of-failure as a reliability driver in power electronics, *IEEE J. Emerg. Sel. Top. Power Electron.* 2 (2014) 97–114.
- [30] F. Blaabjerg, Y. Yang, K. Ma, X. Wang, Power electronics - the key technology for renewable energy system integration, in: 2015 International Conference on Renewable Energy Research and Applications (ICRERA), 2015, pp. 1618–1626, <http://dx.doi.org/10.1109/ICRERA.2015.7418680>.
- [31] S. Peyghami, P. Davari, F. Blaabjerg, System-level reliability-oriented power sharing strategy for DC power systems, *IEEE Trans. Ind. Appl.* 55 (2019) 4865–4875.
- [32] D. Zhou, H. Wang, F. Blaabjerg, Mission profile based system-level reliability analysis of DC/DC converters for a backup power application, *IEEE Trans. Power Electron.* 33 (2018) 8030–8039.
- [33] S. Peyghami, Z. Wang, F. Blaabjerg, A guideline for reliability prediction in power electronic converters, *IEEE Trans. Power Electron.* 35 (2020) 10958–10968.
- [34] H. Mahmood, D. Michaelson, J. Jiang, Strategies for independent deployment and autonomous control of PV and battery units in islanded microgrids, *IEEE J. Emerg. Sel. Top. Power Electron.* 3 (3) (2015) 742–755.
- [35] S. Piller, M. Perrin, A. Jossen, Methods for state-of-charge determination and their applications, *J. Power Sources* 96 (2001) 113–120.
- [36] M.A.G.d. Brito, L.P. Sampaio, G. Luigi, G.A.e. Melo, C.A. Canesin, Comparative analysis of MPPT techniques for PV applications, in: 2011 International Conference on Clean Electrical Power (ICCEP), 2011, pp. 99–104, <http://dx.doi.org/10.1109/ICCEP.2011.6036361>.
- [37] E. Schaltz, A. Khaligh, P.O. Rasmussen, Influence of battery/ultracapacitor energy-storage sizing on battery lifetime in a fuel cell hybrid electric vehicle, *IEEE Trans. Veh. Technol.* 58 (2009) 3882–3891.
- [38] D.U. Sauer, H. Wenzl, Comparison of different approaches for lifetime prediction of electrochemical systems Using lead-acid batteries as example, *J. Power Sources* 176 (2008) 534–546.
- [39] R. Bayerer, T. Herrmann, T. Licht, J. Lutz, M. Feller, Model for power cycling lifetime of IGBT modules - various factors influencing lifetime, in: 5th International Conference on Integrated Power Electronics Systems, 2008, pp. 1–6.
- [40] P. Asimakopoulos, K. Papastergiou, T. Thiringer, M. Bongiorno, G.L. Godec, On SV_\texttt{method}: In situ temperature estimation and aging detection of high-current IGBT modules used in magnet power supplies for particle accelerators, *IEEE Trans. Ind. Electron.* 66 (2019) 551–560, <http://dx.doi.org/10.1109/TIE.2018.2823689>.
- [41] M. Musallam, C.M. Johnson, An efficient implementation of the rainflow counting algorithm for life consumption estimation, *IEEE Trans. Reliab.* 61 (2012) 978–986, <http://dx.doi.org/10.1109/TR.2012.2221040>.
- [42] R.N. Allan, et al., Reliability Evaluation of Power Systems, Springer Science & Business Media, 2013.
- [43] R. Billinton, R.N. Allan, Reliability Evaluation of Engineering Systems, Springer, 1992.
- [44] S. Peyghami, F. Blaabjerg, P. Palensky, Incorporating power electronic converters reliability into modern power system reliability analysis, *IEEE J. Emerg. Sel. Top. Power Electron.* 9 (2021) 1668–1681, <http://dx.doi.org/10.1109/JESTPE.2020.2967216>.
- [45] S. Peyghami, M. Fotuhi-Firuzabad, F. Blaabjerg, Reliability evaluation in microgrids with non-exponential failure rates of power units, *IEEE Syst. J.* 14 (2) (2019) 2861–2872.